JOURNAL OF SOLID STATE CHEMISTRY **133,** 529–535 (1997)
ARTICLE NO. SC977527

Second-Harmonic Generation of Electrically Poled Borophosphate Glasses: Effects of Introducing Niobium or Sodium Oxides

V. Nazabal,[1] E. Fargin, J. J. Videau, and G. Le Flem

ICMCB (UPR 8661, CNRS), Chateau Brivazac, Avenue du Dr Schweitzer, 33608 Pessac Cedex, France

A. Le Calvez, S. Montant, E. Freysz, and A. Ducasse

CPMOH (URA CNRS 283), Université de Bordeaux I, 351 Cours de La Libération, 33405 Talence Cedex, France

and

M. Couzi

Laboratorie de Spectroscopie Moléculaire et Cristalline (URA CNRS 124), Université de Bordeaux I, 351 Cours de La Libération, 33405 Talence Cedex, France

Received March 27, 1997; accepted June 29, 1997

Second-harmonic generation in poled glasses opens new frontiers in optical material research. Within this context new borophosphate glasses of the $Ca(PO_3)_2$–CaB_4O_7–$Na_2B_4O_7$–Nb_2O_5 system were synthesized and their second-harmonic generation was evaluated after poling treatment. The enhancement of the second-harmonic signal with niobium oxide content is related to the presence of distorted NbO_6 octahedra in the former of the glasses and to the increase in third-order susceptibility. The intensity of the measured second-harmonic signal is not dependent on the amount of sodium (100–1000 ppm) introduced into the glass.

INTRODUCTION

Nonlinear optical properties of transparent materials are the focus of growing interest for the elaboration of all-optical devices, such as photonic modulators, optical data storage devices, and telecommunication devices, or for the spectral extension of laser sources. Generally speaking, the nonlinear optical properties of materials under an electromagnetic field E result from the generation of a polarization P, which can be expressed as a power series in E,

$$P = \chi^{(1)}E + \chi^{(2)}E\cdot E + \chi^{(3)}E\cdot E\cdot E + \ldots,$$

where $\chi^{(1)}$ is the linear susceptibility which accounts for the linear index, and $\chi^{(2)}$ and $\chi^{(3)}$ correspond respectively to the second- and third-order nonlinear susceptibilities. In glasses, the macroscopic inversion symmetry implies $\chi^{(2)} = 0$. Nevertheless, second-harmonic generation (SHG) was observed in bulk glasses submitted to a poling treatment (1). This technique consists of applying a direct-current (dc) electric field below the glass transition temperature (T_g) and cooling the glass before removing the dc bias. The materials reportedly involved are mainly SiO_2- and TeO_2-based bulk oxide glasses (1–5). According to Myers *et al.*, two different mechanisms can account for the induced second-order susceptibility (1, 2):

$$\chi^{(2)} = \chi^{(3)}E_{dc} + \sum (Np\beta/5kT)E_{loc}. \qquad [1]$$

The first term is related to the electrical field-induced second-order process. The second term is the induced macroscopic second-order nonlinearity resulting from reorientation by the local field E_{loc} of polar bonds, which have a permanent dipole moment p and a hyperpolarizability β. The phenomena able to induce such fields E_{loc} and E_{dc} have been related to migration of mobile ions, e.g., Na^+, toward the cathode face. It is important to note that Eq. [1] indicates the important physical parameters that control the amplitude of the induced second-order susceptibility. Although the methods of elaboration of the glass and the poling parameters have been shown to modify the measured second-harmonic (SH) intensity (6–9), few experiments have checked the influence of the chemical composition of the glass on the poling process and on the induced $\chi^{(2)}$ (4, 5, 10–12).

This paper reports SHG experiments performed on poled sodium-doped calcium borophosphate glasses containing

[1]To whom correspondence should be addressed. Fax: 05 56 84 27 61. E-mail: nazabal@chimsol.icmcb.u-bordeaux.fr.

0022-4596/97 $25.00

various proportions of niobium oxide. Our first aim was to understand the effect of Na^+ ions on the poling process, since an electrical breakdown is often observed in glasses with a rich content of sodium oxide. By introducing niobium oxide, our second aim was to improve both the $\chi^{(3)}$ susceptibility of the material and the proportion of highly polarizable entities in the glasses (13).

The compositions of the glasses can be expressed by the general formula $(1-y)[0.9Ca(PO_3)_2,\ (0.1-x)CaB_4O_7$–$xNa_2B_4O_7]yNb_2O_5$, where $y = 0,\ 0.1,\ 0.2$ and $x < 0.01$. The $0.95NaPO_3$–$0.05Na_2B_4O_7$ glass matrix had previously been studied and proven to be perfectly transparent between 300 and 1600 nm for large quantities of strongly polarizable Nb_2O_5 without crystallization (13, 14). As an electrical breakdown is always induced during the poling treatment for high sodium content, it is necessary to replace the majority of sodium with calcium and to control the amount of sodium by introducing small quantities of $Na_2B_4O_7$. In view of this, the $0.9Ca(PO_3)_2$–$0.1CaB_4O_7$ glass matrix was selected instead of the previously studied $0.95NaPO_3$–$0.05Na_2B_4O_7$ matrix, for similar P/B ratio. Then, the influence of controlled amounts of Na doping and addition of niobium oxide on the poling process and the induced SHG nonlinearity were studied.

EXPERIMENTAL

1. Sample Preparation

The starting chemical reagents were commercial powders of Nb_2O_5, $(NH_4)_2HPO_4$, $CaCO_3$, and B_2O_3 with a purity higher than 99.9%. Calcium metaphosphate, $Ca(PO_3)_2$, was synthesized by thermal treatment of an appropriate mixture of $(NH_4)_2HPO_4$ and $CaCO_3$ powders. Long periods ($\sim$15 h) at 300 and 850°C were necessary to avoid frothing of the products. The purity of $Ca(PO_3)_2$ was checked by X-ray diffraction. Stoichiometric proportions of Nb_2O_5, $Ca(PO_3)_2$, B_2O_3, and $CaCO_3$ were then mixed and heated for 15 h at 700 °C in a furnace under oxygen atmosphere. The mixture was ground with additional small quantities of $Na_2B_4O_7$ (99.99% in purity) to adjust the required concentration of sodium. It was then melted at 1350°C, quenched between two plates of graphite, and annealed overnight under oxygen atmosphere at 20°C below the glass transition temperature. The prepared glasses were colorless and transparent, and became slightly yellow but transparent at a Nb_2O_5 content of 20 mol%. The actual compositions of the as-prepared glasses are given in Table 1. All samples were cut into approximately $10 \times 10 \times 1.5$-mm plates and the surfaces were carefully polished.

2. Poling Technique

The glass plates, about 1.5 mm thick, were inserted between two plane brass electrodes and heated to about 300°C. Then a dc bias of 2.7 kV was applied across the sample for 5 h. The temperature was slowly decreased while the applied voltage was held constant. The dc bias was then removed. The effect of the poling can be suppressed by heating the poled glasses at 400 °C in a furnace for 1 h in the absence of an external electrical field. Good contact between

TABLE 1
Compositions of the Doped Sodium Borophosphate Glasses Containing Various Proportions of Niobium Oxide

Glasses	P (w%)		B (w%)		Ca (w%)		Nb (w%)		Na (ppm)
	Calc.	Anal.	Calc.	Anal.	Calc.	Anal.	Calc.	Anal.	
Matrix $0.9Ca(PO_3)_2$–$0.1CaB_4O_7$	28.2	27.4	2.2	1.96	20.3	20.64	0	0	103
10% Nb_2O_5 $0.9(0.9Ca(PO_3)_2$–$0.1CaB_4O_7)$: $0.1Nb_2O_5$	24.5	24.8	1.9	1.82	17.6	17.68	9	8.48	170
10% Nb_2O_5 $0.9(0.9Ca(PO_3)_2$–$(0.1-x)CaB_4O_7$–$xNa_2B_4O_7)$:$0.1Nb_2O_5$	24.5	24.21	1.9	1.74	17.6	18.56	9	9.19	465
10% Nb_2O_5 $0.9(0.9Ca(PO_3)_2$–$(0.1-x)$ CaB_4O_7–$xNa_2B_4O_7)$:$0.1Nb_2O_5$	24.5	23.5	1.9	1.86	17.6	17.86	9	9.77	820
10% Nb_2O_5 $0.9(0.9Ca(PO_3)_2$–$(0.1-x)CaB_4O_7$ $-xNa_2B_4O_7)$:$0.1Nb_2O_5$	24.5	24.4	1.9	1.83	17.6	18.18	9	8.7	1300
20% Nb_2O_5 $0.8(0.9Ca(PO_3)_2$–$0.1CaB_4O_7)$: $0.2Nb_2O_5$	21.1	21.2	1.6	1.51	15.17	14.95	17.6	18.40	116

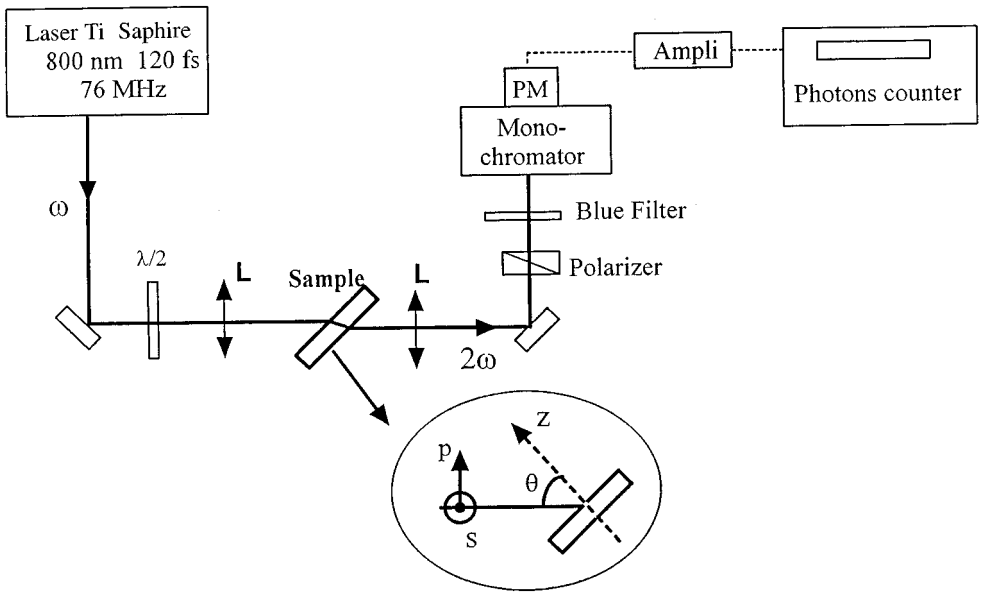

FIG. 1. SHG experimental setup. The inset shows the *s* and *p* polarizations.

the electrodes and the glass plate resulted in an improvement in the recorded SH signals.

3. *Characterizations*

The glass transition (T_g) and crystallization (T_c) temperatures have been accurately measured (standard deviation $<5°C$) using DSC apparatus (Seiko Instruments Inc.). The heating rate was 600°C/h in the range 30–1000°C.

The densities were measured by immersing the samples in calibrated diethylorthophthalate. The accuracy was better than 0.3%.

UV–visible absorption spectra were recorded between 250 and 1500 nm, at room temperature, using a Cary 2415 spectrophotometer (Varian). The spectra were normalized to a 1-mm thickness for all samples.

The Raman spectra were recorded on a Dilor Z24 triple monochromator. The 514.5-nm laser line of a Spectra Physica Model 2030 argon ion laser was used for excitation with an incident power of 200 mW. The signal was detected using a Hamamatsu cooled photomultiplier coupled to a photon counting system. The spectral resolution was about 2 to 3 cm^{-1}.

The setup for the SHG measurement is presented in Fig. 1. A continuous mode-locked, linearly polarized Ti:sapphire laser system (Coherent Mira 900) delivers pulses of 120 fs at a 76-MHz repetition rate around 800 nm and at about 10–kW peak power. The SH signal was measured in transmission through the poled glasses. The fundamental radiation was removed by a colored glass filter and a monochromator. The SH signal was recorded with a photomultiplier coupled to a photon counting system. The poled glasses are expected to have $C_{\infty V}$ symmetry. Then if the *z* axis, chosen to be the direction of the applied electrical field, is in the plane of incidence, only a *p*-polarized SH signal is generated when the angle of incidence $\theta \neq 0°$ (Fig. 1). The results collected in Fig. 2 are in good agreement with this symmetry. The *s* component of the SH signal is 10^3 to 10^4 lower than the *p* component.

The linear indices and third-order hyperpolarizabilities, $\chi^{(3)}_{xxxx}$, were measured in a time-resolved optical Kerr experiment (15). Calibration of the Kerr effect signal was carried out with a sample of commercial SF59 glass for which the $\chi^{(3)}_{xxxx}$ value is known to be 6.5×10^{-21} m^2 V^{-2} (16). The conventions used for $\chi^{(3)}_{xxxx}$ are those proposed by Butcher and Cotter (17).

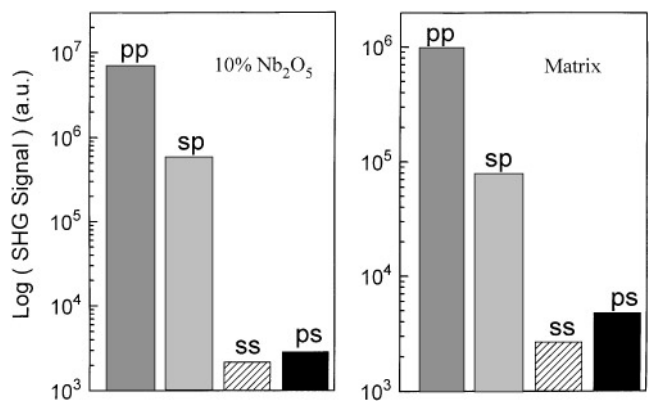

FIG. 2. SHG signal for different configurations of pump and second-harmonic beam polarizations. For instance, *sp* corresponds to a *s*-polarized fundamental beam and a *p*-polarized harmonic beam.

TABLE 2

Glass Transition Temperature (T_g), Recrystallization Temperature (T_c), and Densities of the Borophosphate Glasses Investigated

Glasses	T_g (°C)	T_c (°C)	$T_g - T_c$ (°C)	ρ (g/cm^3)
Matrix	600	724	124	2.71
10% Nb_2O_5	636	764	128	2.90
20% Nb_2O_5	660	800	140	3.09

RESULTS AND DISCUSSION

1. Thermal Properties and Densities

Thermal parameters and densities are listed in Table 2. T_g and T_c increase with the proportion of niobium oxide in the borophosphate glass matrix. However, the T_g–T_c remains constant for 10 or 20 mol% Nb_2O_5. The densities of glasses increase with niobium oxide content, as was observed for the sodium borophosphate glasses (13).

2. Structural Properties

The parallel (vv) polarized Raman spectra of the glasses investigated are illustrated in Fig. 3. The spectrum of the niobium-free glass [$x = 0$, $B/(B + P) = 0.182$] can be analyzed by comparison with the spectra of the vitreous $Ca(PO_3)_2$ and of the homologous $0.95NaPO_3$–$0.05\,Na_2B_4O_7$ glass [$B/(B + P) = 0.173$] (13, 18–20), called NaPB subsequently in the text. The assignments of the Raman lines of these two glasses are listed in Table 3 for comparison. The networks of the $Ca(PO_3)_2$ and NaPB glasses are composed of variable-length chains of corner-sharing PO_4 tetrahedra leading to the formation of P–O–P bonds. The corresponding Raman spectral bands are typical of the metaphosphate structure at about 1270 cm^{-1} [$\nu_{as}(PO_2^-)$], 1150 cm^{-1} [$\nu_s(PO_2^-)$], and 690 cm^{-1} [ν_s(POP)]. In NaPB glass, the boron atoms form tetrahedral BO_4^{2-} units branching to phosphate chains. Accordingly, additional lines corresponding to $\nu_s(PO_2^-)$ vibrations in phosphate units connected to boron atoms appear as shoulders on the major bands (19, 20). Simultaneously, ν(POB) stretching modes give two lines on each side of the large ν_s(POP) band.

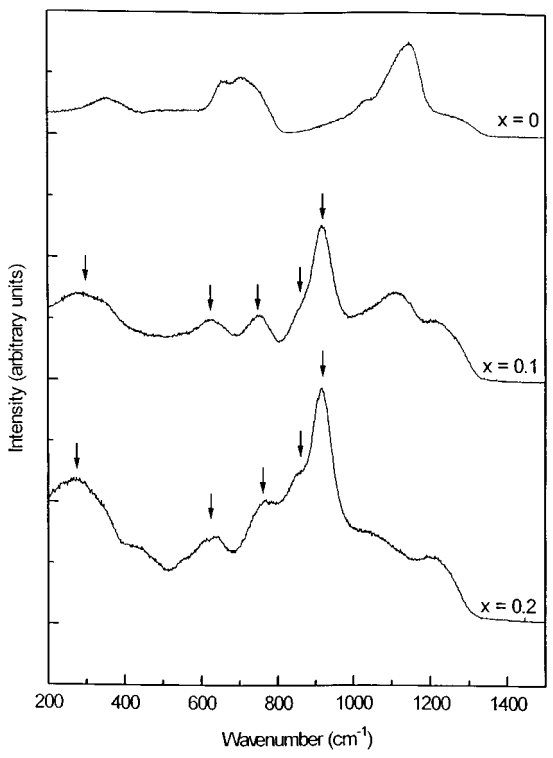

FIG. 3. Raman spectra of glasses of compositions $(1 - x)$ $[0.9Ca(PO_3)_2$–$0.1CaB_4O_7]$–xNb_2O_5, where $x = 0$, 0.1, and 0.2. The arrows indicate the bands due to the introduction of Nb_2O_5.

TABLE 3

Position and Assignment of Raman Lines of the Calcium Borophosphate Glass ($x = 0$), Vitreous Form $Ca(PO_3)_2$, and the Glass of Composition $0.95NaPO_3$–$0.05Na_2B_4O_7$

Frequency (cm^{-1})			
$Ca(PO_3)_2$ (18)	NaPB (19, 20)	Matrix ($x = 0$)	Band vibration assignment
1274 m[a]	1260 m	1253 m	$\nu_{as}PO_2^-$
1150 s	1150 s	1144 s	$\nu_sPO_2^-$
	1070 m	1060 m	$\nu_sPO_2^-$
			shoulder due to the presence of boron atoms
	1040 m	1032 m	$\nu_sPO_2^-$
			shoulder due to the presence of boron atoms
	760 m	750 m	ν_sPOP
780 m and 693 s	700 s	706 s	ν_sPOP
	640 m	660 s	ν_sPOB

[a] m, medium; s, strong.

The spectrum of the niobium-free calcium borophosphate glass investigated ($x = 0$ in Fig. 3) is dominated by three broad bands centered at 1144, 706, and 660 cm^{-1} and smaller lines at 1253, 1060, 1032, and 750 cm^{-1}. According to the assignments reported in Table 3, the line at 1144 cm^{-1} and the shoulder at 1253 cm^{-1} are respectively typical of the $\nu_s(PO_2^-)$ and $\nu_{as}(PO_2^-)$ vibration modes. The shoulders around 1032 and 1060 cm^{-1} may also be assigned to $\nu_s(PO_2^-)$ vibrations in phosphate units connected to boron atoms. In the lower frequency range, the band with a maximum at 706 cm^{-1} is due to the ν_s(POP) stretch in phosphate chains, and the shoulder at 660 cm^{-1} is attributed to ν_s(POB) stretching modes. In addition, the absence of the $\nu_s(BO^-)$ stretching mode in the frequency

domain 1300–1500 cm^{-1} involving nonbridging oxygen atoms in BO_3 units allows us to conclude that the boron atoms are surrounded by bridging oxygen atoms in fourfold coordination as in the sodium borophosphate glasses.

The introduction of Nb_2O_5 induces the appearance of very strong lines (indicated by the arrows in Fig. 3) peaking at 916 cm^{-1} with new smaller bands close to 850, 750, 630, 420, and 270 cm^{-1}. This evolution was previously discussed in the case of sodium phosphate and borophosphate glasses (13, 21). The new bands are characteristic of the presence of niobium in sixfold coordination. The line at 916 cm^{-1} is typical of a very distorted octahedron with a short apical Nb–O bond. The bands between 500 and 800 cm^{-1} are related to the existence of bridging oxygen atoms in the Nb–O–Nb entities. The appearance of a shoulder at 850 cm^{-1} for $x = 0.2$ suggests the formation of corner-shared NbO_6 octahedra, possibly in the form of chains, with the presence of alternate short and long Nb–O bonds.

In conclusion, the introduction of increased amounts of Nb_2O_5 into calcium borophosphate initially breaks down the ramified borophosphate glass structure and progressively develops a new mixed network former consisting of entities of NbO_6 octahedra. These share common corners similar to those found in sodium borophosphate glasses (13). This structural description is consistent with the increase in the measured density with niobium content.

3. Optical Properties

i. Transmission spectra. Figure 4 shows the transmission spectra of the glasses investigated between 200 and 1500 nm. After subtraction of the Fresnel reflection, almost perfect transmittance is observed from the visible to the near-infrared regions. Cutoff wavelengths and corresponding cutoff energies are given in Table 4. The latter parameters slightly decrease with niobium concentration but remain in the near-UV domain. The origin of this absorption can be understood in terms of the transition between orbitals mostly localized on oxygen and antibonding orbitals mostly localized on niobium. As previously reported for niobium phosphate or borophosphate glasses (13, 21), the progressive clustering of NbO_6 octahedra corresponds to a red shift in the cutoff wavelength. In view of this it is interesting to make a comparison with the limiting case of pure niobium oxide $NaNbO_3$ of perovskite type, for which the absorption threshold occurs at 3.29 eV (21): this value can be considered as a typical limit of a three-dimensional arrangement of NbO_6 octahedra sharing common corners. Therefore, the evolution of the cutoff energy with respect to glass composition is consistent with the growth of a new mixed network former described previously.

TABLE 4

Cutoff Energies (E_c) and Corresponding Wavelengths (λ_c) of the Transmission Spectra of $(1-y)(0.9Ca(PO_3)_2$–$0.1CaB_4O_7)$: yNb_2O_5 ($y = 0$, 0.1, 0.2) Glasses

Sample	E_c (eV)	λ_c (nm)
Matrix	5.2	236
10% Nb_2O_5	4	312
20% Nb_2O_5	3.8	324

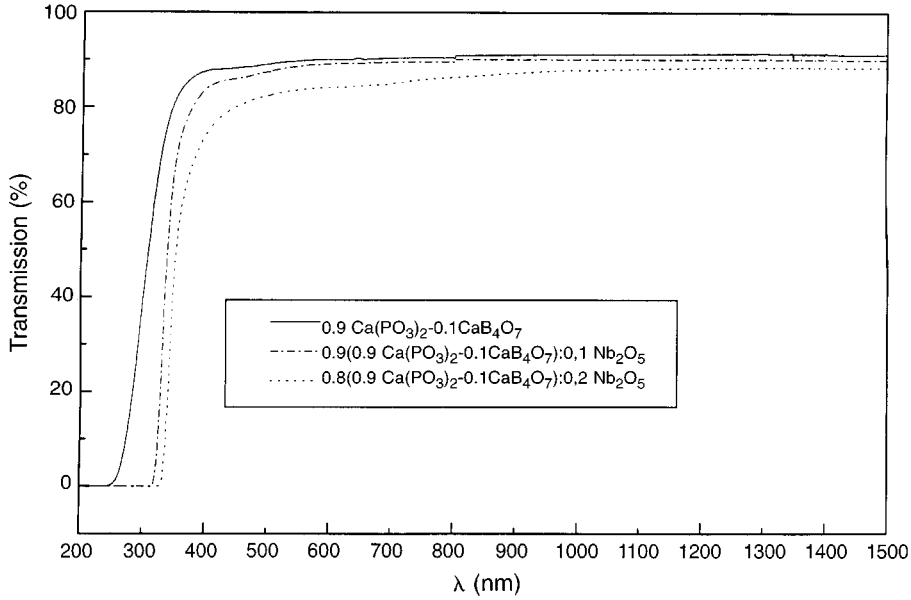

FIG. 4. UV–visible transmission spectra of the borophosphate samples investigated.

TABLE 5
Linear Indices n_0 and Cubic Susceptibilities $\chi^{(3)}_{xxxx}$ of the Studied Borophosphate Glasses Calibrated against SF59

Glasses	Nb_2O_5 (mol/cm^3)	n_0	$\chi^{(3)}$ (10^{-21} m^2 V^{-2})
Matrix	0	1.56	0.39
10% Nb_2O_5	$1.84 * 10^{-3}$	1.61	0.78
20% Nb_2O_5	$2.9 * 10^{-3}$	1.67	1.2
SF59	0	1.985	6.5

ii. Third-order nonlinear optical properties. The intensity of the third-order nonlinear response increases with niobium concentration (Table 5), as was previously reported for sodium borophosphate glasses (13). In this range of niobium concentration the order of magnitude of $\chi^{(3)}$ agrees with the expected values calculated on the basis of bond orbital theory introduced by Lines for dielectric crystals (22) and recently applied to glasses (16, 23). The increase in $\chi^{(3)}$ resulting from the progressive introduction of $4d^0$ Nb(V) ions is essentially explained by the contribution of the $4d$ orbital to the linear or nonlinear response, assuming a mean Nb–O distance of about 2 Å.

iii. Second-harmonic generation experiments. The results of SHG experiments are listed in Table 6. The SH signals generated by a SiO_2 commercial glass (Vitreosil) are compared with the signals given by the borophosphate glasses poled under the same conditions. The induced glass matrix nonlinearity $\chi^{(2)}$ is roughly estimated to be about 10 times lower than that of the fused Vitreosil silica $\chi^{(2)}$. This clearly indicates that glass formers other than SiO_2 and TeO_2 can produce a second-order nonlinearity. The reproducibility of the SHG measurements has been tested. For instance, the SH signals of both the glass matrix (No. 1) and one of the most efficient samples (No. 2) were almost constant after a "poling–depoling–poling" cycle. On the other hand, the SHG efficiencies were almost the same for samples of the same composition issued from the same batch (Nos. 5 and 6) or prepared at two different times (Nos. 7 and 8).

TABLE 6
Second-Harmonic Generation Intensity Recorded on Different Samples Poled at 300°C and 2.7 kV

No.	Sample		Time of poling (h)	pp SHG signal (a.u.)
0	Fused Vitreosil silica		1	100
1	Matrix	106 ppm	5	1
			depoled	0
			1	2
2	10% Nb_2O_5	170 ppm Na^+	5	10
			dopled	0
			1	12
3	10% Nb_2O_5	465 ppm Na^+	5	4
4	10% Nb_2O_5	820 ppm Na^+	5	5
5	10% Nb_2O_5	1300 ppm Na^+	5	10
6	10% Nb_2O_5	1300 ppm Na^+	5	13
7	20% Nb_2O_5	116 ppm Na^+	5	13
8	20% Nb_2O_5	116 ppm Na^+	5	9

For a 10% niobium content in borophosphate glasses (samples 2–6), in the limit of experimental uncertainty, the SH signal is weakly dependent on the concentration of sodium in the glass, which has been varied from 100 to 1000 ppm.

The introduction of Nb_2O_5 into the borophosphate matrix increases the SH signal. The saturation of the measured signal between 10 and 20% Nb_2O_5 is probably related to the increase in the absorption at 400 nm recorded on the 20% Nb_2O_5. The $\chi^{(2)}$ of these two glasses is estimated at about 35% of the fused Vitreosil silica nonlinearity.

The localization of the induced nonlinearity was probed within the sample. This was done by propagating the fundamental beam parallel to the anode or cathode surface along the thermally poled glass (Fig. 5). No SH signal was recorded unless the pump beam was focused into the butt end close to the anodic surface of the glass plate. This result, which is in good agreement with Kazansky's observation for a fused silica sample (24), provides evidence of a nonlinearity localized close to the anodic surface. However, this result questions the results of Tanaka *et al.* (3, 12), who deduced from a Maker fringes experiment that the nonlinearity in their tellurite glasses was induced in the whole volume of the sample. The presence of Maker fringes does not imply such a localization. Indeed a nonlinearity induced close to both the anodic and cathodic surfaces would also result in a Maker fringes pattern.

Finally, nonexponential decay of the second harmonic light with respect to time has been recorded on all Nb_2O_5-doped borophosphoniobate glasses (Fig. 6). The decay time depends on the Nb_2O_5 content: the higher the niobium oxide, the faster the decay. This evolution also seems to be related to the increase in absorption at 400 nm with increasing niobium oxide content. This behavior has recently been

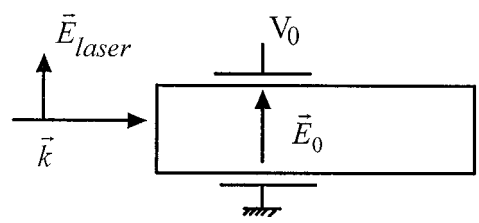

FIG. 5. Experimental SHG configuration to probe the localization of the induced nonlinearity. The fundamental beam propagates perpendicularly to the poling applied field.

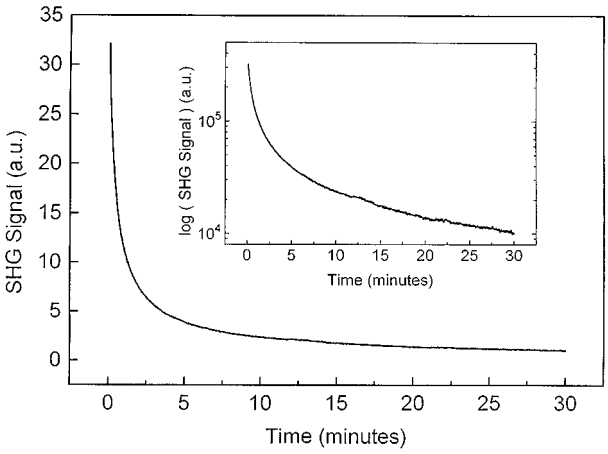

FIG. 6. Nonexponential decay of the SH signal recorded for 20% Nb_2O_5 borophosphate glass.

confirmed by the study of a new 30% Nb_2O_5 borophosphate glass which has exhibited both an increase in this absorption and a faster SH signal decay (25).

CONCLUSION

Second-harmonic generation was studied in electrically poled borophosphate glasses of composition $(1-y)$ [0.9 $Ca(PO_3)_2$, $(0.1-x)CaB_4O_7$–$xNa_2B_4O_7$]yNb_2O_5, where $y = 0$, 0.1, 0.2 and $x < 0.01$. These new borophosphate glasses can be described as composed of limited metaphosphate chains connected by BO_4 tetrahedral groups. Within this former network, the niobium is located in distorted octahedral sites which tend to cluster as the niobium concentration increases. These structural features explain (1) the red shift of the cutoff energy near the UV range of the absorption spectra and (2) the magnitude of the third-order nonlinear response, which is consistent with the approach of the bond orbital theory.

This paper demonstrates clearly that the appearance of SHG in glasses after poling is not restricted to the silica or tellurite system but can be extended to other oxide glasses. In the glasses investigated the sodium concentration had no influence on SHG intensity. In contrast, the introduction of niobium oxide strongly enhanced the performance of the glass. This evolution indicates a correlation between the second-order generated signal and either the cubic susceptibility or the presence of highly distorted NbO_6 entities with high microscopic second-order hyperpolarizabilities. Finally, the SH signal is localized close to the anodic surface. The origin of this phenomenon remains an open question. In future investigations it would be interesting to compare glasses exhibiting glass transition temperatures close to and further from the poling temperature.

REFERENCES

1. R. A. Myers, N. Mukherjee, and S. R. J. Brueck, *Opt. Lett.* **16,** 1732 (1991).
2. N. Mukherjee, R. A. Myers, and S. R. J. Brueck, *J. Opt. Soc. Am. B* **11,** 665 (1994).
3. H. Nasu, J. Matsuoka, and K. Kamiya, *J. Non-Cryst. Solids* **178,** 23 (1994).
4. K. Tanaka, K. Kashima, K. Hirao, N. Soga, A. Mito, and H. Nasu, *Jpn. J. Appl. Phys.* **32,** 843 (1993).
5. K. Tanaka, K. Kashima, K. Hirao, N. Soga, A. Mito, and H. Nasu, *J. Non-Cryst. Solids* **185,** 123 (1995).
6. K. Tanaka, K. Kashima, K. Hirao, N. Soga, S. Yamagata, A. Mito, and H. Nasu, *Jpn. J. Appl. Phys.* **34,** 175 (1995).
7. L. J. Henry, A. D. De Vilbis, and T. E. Tsai, *J. Opt. Soc. Am. B* **12,** 2037 (1995).
8. H. Nasu, H. Okamoto, K. Kurachi, J. Matsuoka, K. Kamiya, A. Mito, and H. Hosomo, *J. Opt. Soc. Am. B* **12,** 644 (1995).
9. H. Takebe, P. G. Kazansky, P. St. Russel, and K. Morinaga, *Opt. Lett.* **21,** 468 (1996).
10. H. Nasu, K. Kurachi, A. Mito, H. Okamoto, J. Matsuoka, and K. Kamiya, *J. Non-Cryst. Solids* **181,** 83 (1995).
11. M. Miyata, H. Nasu, A. Mito, K. Kurachi, J. Matsuoka, and K. Kamiya, *Jpn. J. Appl. Phys.* **34,** L1455 (1995).
12. K. Tanaka, A. Narazaki, K. Hirao, and N. Soga, *J. Non-Cryst. Solids* **203,** 49 (1996).
13. T. Cardinal, E. Fargin, G. Le Flem, M. Couzi, L. Canioni, P. Segonds, L. Sarger, A. Ducasse, and F. Adamietz, *Eur. J. Solid State State Inorg. Chcm.* **33,** 597 (1996).
14. J. F. Ducel and J. J. Videau, *Mater. Lett.* **13,** 271 (1992).
15. A. Le Calvez, S. Montant, E. Freysz, A. Ducasse, X. W. Zhung, and Y. R. Shen, *Chem. Phys. Lett.* **258,** 620 (1996).
16. T. Cardinal, thesis, Université de Bordeaux I, January 1997.
17. P. N. Butcher and D. Cotter, "The Elements of Nonlinear Optics." Cambridge Univ. Press, London/New York, 1990. The polarization at the frequency ω is $P_\omega(r,t) = K\chi^{(3)}(\omega, -\omega, \omega)A_\omega(r,t)\ A^*_\omega(r,t)A_\omega(r,t)$, with $E_\omega(r,t) = \frac{1}{2}(A_\omega(r,t)\exp(i(\omega t - kr)) + A^*_\omega(r,t)\ \exp(-i(\omega t - kr)))$ and the same for $P_\omega(r,t)$. For our degenerated optical Kerr effect experiment, $K = 3/2$.
18. J. E. Pemberton, L. Latifzadeh, J. P. Fletcher, and S. H. Risbud, *Chem. Mater.* **3,** 195 (1991).
19. J. F. Ducel, J. J. Videau, and M. Couzi, *Phys. Chem. Glasses* **34,** 212 (1993).
20. J. F. Ducel, J. J. Videau, and M. Couzi, *Phys. Chem. Glasses* **35,** 253 (1994).
21. A. El Jazouli, J. C. Viala, C. Parent, G. Le Flem, and P. Hagenmuller, *J. Solid State Chem.* **73,** 433 (1988).
22. M. E. Lines, *Phys. Rev. B* **43,** 11978 (1991).
23. S. Le Boiteux, P. Segonds, L. Canioni, L. Sarger, T. Cardinal, C. Duchesne, E. Fargin, and G. Le Flem, *J. Appl. Phys.* **81,** 1481 (1997).
24. P. G. Kazansky and P. St. J. Russel, *Opt. Commun.* **110,** 611 (1994).
25. V. Nazabal, E. Fargin, and G. Le Flem, *in* "Proceedings, Miniature Coherent Light Sources in Dielectric Media, Les Houches, 1–6 June 1997."